THE CORRELATION BETWEEN MECHANICAL STRUCTURE AND MICRO-CHANNELS IN THERMAL ENERGY STORAGE SYSTEMS

by

Wei SUN*

Department of Mechanical Engineering,
Anhui Technical College of Mechanical and Electrical Engineering, Wuhu, Anhui, China

Original scientific paper
https://doi.org/10.2298/TSCI2506197S

Aiming to address the challenge of optimizing the heat transfer performance of micro-channels and the mechanical structure strength in thermal energy storage systems in a co-ordinated manner, this paper proposes a bionic coupling structure design and establishes a multi-physics field coupling model. The study analyzes the heat transfer and mechanical properties of rectangular, circular, and triangular micro-channels, constructs a comprehensive performance evaluation index ξ, and determines the correlation between the depth-to-width ratio and the maximum allowable deformation. The bionic fractal tree-like micro-channel structure (Scheme C) exhibits a heat transfer efficiency of 89.7% under medium load conditions, which is 14.1% higher than that of the traditional parallel channel (Scheme A). The maximum stress is reduced by 12.2%, and the pressure loss is controlled at 5.4 kPa. After the improved model introduces the mesoscopic effect correction, the heat transfer calculation error of the 50 μm channel is reduced from 12.5% to 2.7%, and the deviation from the experimental data is ≤1.2%. Experimental verification shows that the design achieves a co-ordinated improvement in heat transfer efficiency and structural strength, providing theoretical support for the efficiency and compactness of thermal energy storage systems.

Key words: *thermal energy storage, micro-channel, force-heat coupling, bionic structure, multi-physics field model, mesoscopic effect*

Introduction

As a key link in balancing energy production and consumption, thermal energy storage technology plays an indispensable role in renewable energy grid integration, industrial waste heat recovery, and other fields. The performance of its system directly depends on two core elements: the long-term stability of the mechanical structure and the efficiency of thermal energy conversion and storage. With its unique high specific surface area characteristics, micro-channels have demonstrated outstanding potential in enhancing heat transfer and have become a crucial technical means to improve the efficiency of thermal energy storage systems. However, most current studies separate the heat transfer performance of micro-channels from the mechanical properties of mechanical support structures for analysis, ignoring the synergistic mechanism of the two under the force-heat coupling in actual operation [1]. This directly leads to the problem that it is difficult to take into account both heat transfer efficiency and structural strength during system integration, which seriously restricts the development of thermal energy storage systems towards high efficiency and compactness [2]. Existing relevant research

* Author's e-mail: andison1997@163.com

data show that even a deviation of 0.1 mm in the cross-sectional size of the micro-channel can cause a fluctuation of up to 15% in the heat transfer efficiency. Once the deformation of the mechanical structure exceeds 5 μm, it will significantly alter the flow field distribution in the micro-channel, thereby affecting the heat transfer effect [3]. Although some scholars have explored the heat transfer characteristics of micro-channels of different shapes, such as rectangles and circles, and some researchers have optimized the strength of mechanical structures such as the shell of the energy storage system, as of now, a quantitative correlation model between micro-channel structural parameters (such as aspect ratio, fin thickness*, etc.*) and mechanical structural mechanical parameters (such as elastic modulus, Poisson's ratio*, etc.*) has not been established. It is impossible to provide accurate theoretical guidance for the optimization design of thermal energy storage systems.

This study proposes constructing a bionic coupling structure to address the aforementioned problems, drawing on the natural mechanism of mechanical and thermal synergy in the honeycomb and beeswax composite system to achieve efficient synergy between micro-channels and mechanical structures [4]. At the same time, a multi-physics field model incorporating mesoscopic slip effects is established to provide a deeper understanding of the dynamic coupling law between micro-channels and mechanical structures. Specifically, the study will clarify the following key issues: Firstly, determine the matching threshold between the hydraulic diameter of the micro-channel and the spacing between the structural supports, and provide parameter basis for the reasonable design of the micro-channel and the mechanical structure. Secondly, propose a correction method for the force-heat coupling coefficient at the mesoscopic scale (characteristic size in the range of 50-500 μm) to improve the simulation accuracy of the model for the actual situation. Size deviations alter flow field uniformity – 0.1 mm narrowing creates 40% higher local velocities, increasing heat transfer fluctuations by 15%. Our coupled model accounts for this. Thirdly, quantify the performance improvement of the bionic structure in terms of heat transfer efficiency and structural strength compared with the traditional parallel channel [5].

Coupling design of mechanical structure and micro-channel

Selection of micro-channel structural parameters

The structural parameters of the micro-channel directly determine its heat transfer performance and mechanical adaptability, which need to be optimized through a multi-parameter collaborative approach. In terms of cross-sectional shape, the right-angle feature of the rectangular channel will produce a flow stagnation zone. When the flow rate is 0.3 m/s, the temperature of the stagnation zone is 8-12 K higher than that of the mainstream zone. The circular channel has the problem of uneven wall shear force distribution, and the ratio of maximum shear force to average shear force can reach 1.8. The vortex formed at the corners of the triangular channel can enhance local heat transfer, and the heat transfer coefficient is 9% higher than that of the rectangular channel at the same flow rate [6]. The study found that when the characteristic size of the micro-channel is in the range of 100-500 μm, its heat transfer enhancement coefficient has a non-linear correlation with the structural flexural strength. For every 100 μm reduction in the characteristic size, the heat transfer coefficient increases by about 12%, but the flexural strength decreases by 8%-10%. To quantify this correlation, the comprehensive performance evaluation index, ξ, is defined:

$$\xi = 0.6 \times \frac{\mathrm{Nu}}{\left(f^{1/3}\right)} + 0.4 \times \frac{\sigma}{\left(\sigma_0\right)} \tag{1}$$

where Nu is the Nusselt number, f – the Fanning friction coefficient, σ – the actual flexural strength, and σ_0 – the ultimate strength of the substrate. Weights from 12 orthogonal tests with thermal engineers prioritizing efficiency (0.6) for energy systems, validated by ξ peaking at $\alpha = 2.2$ where both metrics balance. This index integrates the heat transfer performance and mechanical stability in a weighted manner [7].

At the same time, the correlation between the micro-channel aspect ratio ($\alpha = h/w$) and the maximum allowable deformation, δ_{max}, is established:

$$\delta_{max} = 5.2 \times 10^{-3} \times \alpha^{-0.7} \times E^{0.3} \times t^{0.8} \tag{2}$$

where E [GPa] is the elastic modulus of the material and t [μm] – the channel wall thickness. When α increases from 1-5, δ_{max} decreases by 67%, indicating that a large aspect ratio will significantly reduce the structural fault tolerance.

Matching design of mechanical structure and micro-channel

The support stiffness of the mechanical structure has a dynamic coupling relationship with the flow field distribution of the micro-channel. When the ratio of the support spacing, L, to the hydraulic diameter, d_h, of the micro-channel exceeds the critical value ($L/d_h > 20$), the flow field disturbance decreases by more than 40%, resulting in a decrease of 12%-15% in heat transfer efficiency. For this purpose, the coupling equation of support stiffness, K, and flow resistance, ΔP, is constructed:

$$\begin{aligned} K &= \frac{E \times w \times t^3}{4 \times L^5} \\ \Delta P &= \frac{32 \times \mu \times u \times L}{\varphi \times d_h^2} \end{aligned} \tag{3}$$

where μ [Pa·s] is the dynamic viscosity of the working fluid, u [ms^{-1}] – the flow rate, and φ – the cross-sectional correction coefficient (0.82 for rectangle). The w is the micro-channel array width (50 mm for the test system), derived from structural blueprints, ensuring $K = 1.2 \cdot 10^4$ N/m matches experimental stiffness measurements.Through simultaneous solution, it is found that when $K = 1.2 \cdot 104$ N/m, ΔP can be controlled within 5 kPa, while satisfying the structural resonance frequency to avoid the working frequency band of 100-500 Hz, avoiding additional energy consumption and structural damage caused by resonance.

In terms of lay-out, the gradient spacing design principle is proposed. Along the mainstream direction, the micro-channel spacing, s, increases linearly according to $s(x) = s_0 \times (1 + 0.05x/L)$. In the case of a particular energy storage system, this design reduces pressure loss by 15% while ensuring that the deviation in heat transfer uniformity is less than 3%. This design can adapt to the thermal deformation of the mechanical structure caused by the temperature gradient [8].

Coupling design scheme

The bionic coupling design draws on the mechanical advantages of the honeycomb hexagonal structure and the transport efficiency of the leaf vein network to propose a fractal tree-like micro-channel structure. Its branching angle, θ:

$$\theta = 25^\circ \times n^{-0.15} \tag{4}$$

where n is the number of branches ($n = 1, 2, 3$), the first branch $\theta = 25°$, the second branch is reduced to 22°, and the third branch is 20°. The relationship between the fractal dimension, D, and the heat transfer area increment, ΔA, is established:

$$\frac{\Delta A}{A_0} = 1.8 \times (D - 1.2) \times \mathrm{Re}^{0.2} \tag{5}$$

When $D = 1.6$, Re = 2000, $\Delta A/A_0$ reaches 1.3 times, while the mass of the structure increases by only 9%, which is 21% lower than the mass of the traditional structure with the same heat transfer area [9].

Construction of multi-physics coupling model

Heat transfer model

The heat transfer model must comprehensively consider the complex heat transfer mechanism within the micro-channel. The thermal relaxation time correction term is introduced to describe the non-Fourier effect at the mesoscopic scale, and the heat conduction equation is corrected to:

$$\frac{\partial T}{\partial t} = \alpha \nabla^2 T + \frac{T_t \partial^2 T}{\partial t^2} \tag{6}$$

where α is the thermal diffusion coefficient and τ_t – the thermal relaxation time 1. $2 \cdot 10^{-7}$ second for air. The τ_t calibrated via 50 μm channel heat pulse tests, matching thermal wave propagation delays (±5%) measured by infrared thermography, improving non-Fourier effect accuracy. This model can accurately capture the thermal wave effect when the temperature gradient in the micro-channel exceeds 10^5 K/m.

In the convective heat transfer calculation, the influence of wall roughness, ε, on the Nusselt number is considered, and a modified correlation is proposed:

$$\mathrm{Nu} = 0.023 \mathrm{Re}^{0.8} \mathrm{Pr}^{0.4} \left(\frac{1 + 4.6\varepsilon}{d_\mathrm{h}} \right) \tag{7}$$

when ε/d_h increases from 0-0.05, the Nusselt number value increases by 27%, which is less than 4% from the experimental measurement results. The radiation heat transfer is calculated using the net radiation method. For high temperature conditions ($T > 400$ K), the wall emissivity variation function $\varepsilon(T) = 0.15 + 0.0003T$ is introduced, which improves the calculation accuracy of the radiation heat flux by 12%.

Fluid dynamics model

For the low Reynolds number (Re < 2000) flow characteristics in the micro-channel, the Navier-Stokes equation is corrected by the slip boundary. The wall slip velocity, u_s, satisfies:

$$u_s = \beta \lambda \left(\frac{\partial u}{\partial y} \right)_v \tag{8}$$

where β is the slip coefficient. The $\beta = 1.2$ for Ra < 0.8 μm (smooth), decreasing to 0.8 for Ra = 5 μm (rough), calibrated via particle image velocimetry, reducing slip velocity error to <3%. The λ is the molecular mean free path, and $(\partial u/\partial y)_v$ is the wall normal velocity gradient. This correction reduces the flow calculation deviation of a 100 μm scale channel from 15% -3%.

In the pressure loss calculation, considering the channel inlet section effect, a local resistance coefficient correction formula is proposed:

$$\zeta = 0.5 + \frac{1.8}{\mathrm{Re}^{0.3}} + \left(\frac{L_e}{L} \right)^2 \tag{9}$$

where L_e is the length of the inlet section. When $L/L_e < 0.5$, this correction can control the pressure loss calculation error within 5%.

Structural mechanics model

The structural mechanics analysis employs an elastic-plastic constitutive model, taking into account the temperature's influence on material properties. The relationship between the elastic modulus and temperature is:

$$E(T) = E_0\left[1 - 0.0002\left(T - T_0\right)\right] \tag{10}$$

where E_0 is the elastic modulus at the reference temperature, T_0. Linear model valid for 300-450 K (Cu), with <2% error *vs*. experimental data. The thermal stress calculation introduces anisotropic correction of the thermal expansion coefficient. For Cu micro-channels, the axial thermal expansion coefficient, α_x, is 8% higher than the radial, α_r, and the material properties need to be defined separately.

Multi-physics coupling model

When establishing the coupling relationship between fields, the coupling between temperature field and stress field is realized through thermal strain: $\varepsilon_n^{th} = \alpha_t \Delta T$, where α_t is the thermal expansion coefficient matrix [10]. The channel section deformation, δ, and flow velocity correction coefficient, k, satisfy:

$$k = 1 - 0.8\left(\frac{\delta}{d_h}\right)^2 \tag{11}$$

When $\delta/d_h = 0.1$, the velocity calculation needs to be corrected by –0.8%. This relationship is obtained by fitting 20 sets of deformation conditions. The coupling solution adopts the iterative relaxation method. The field variable transfer coefficient is updated in each iteration. The convergence criterion is set as the variable change in adjacent iteration steps is less than 10^{-4}.

Model improvement

Given the comprehensive influence of mesoscopic scale effects, a multi-field coupling correction factor, n, is introduced:

$$\eta = \exp\left[-0.6\left(\frac{d_p}{\lambda}\right)^{-0.7}\right] \tag{12}$$

It is embedded in the source term of the momentum equation and the energy equation. When $d_A/\lambda < 20$, the η value drops from 1-0.3, which effectively corrects the deviation of the continuous medium assumption. The d_p = micro-channel hydraulic diameter, ensuring η corrects continuous medium assumptions when $d_p/\lambda < 20$, reducing error to 2.7%.

Simulation experiment design and result analysis

Simulation parameter setting

The simulation boundary conditions are set according to three typical working conditions: low load (inlet temperature 300 K, flow rate 0.1 m/s), medium load (353 K, 0.5 m/s), and high load (400 K, 1.0 m/s).The outlet is assumed to be a free flow at normal pressure [11]. The mechanical structure features a combination of fixed constraints (bottom) and hinged con-

straints (sides), with an initial temperature of 298 K. The calculation parameters are set time step $1 \cdot 10^{-4}$ second, iterative convergence residual $1 \cdot 10^{-6}$, and a total number of grids of 860000. The SIMPLEC algorithm is used to solve the pressure-velocity coupling.

Simulation based on improved model

Three design schemes were simulated and compared: traditional parallel channels (Scheme A), staggered channels (Scheme B), and bionic fractal channels (Scheme C). The simulation results show that Scheme C performs best under medium load conditions, with an outlet temperature 8.3 K lower than that of Scheme A and a pressure loss 21% lower than that of Scheme B. Table 1 shows the performance parameter comparison of the three schemes (medium load conditions). Fractal branches create multi-stage heat sinks, increasing surface area by 30% and reducing boundary-layer thickness by 40%, boosting efficiency *vs*. Scheme B single-path flow.

Table 1. Comparison of performance parameters of three schemes (medium load condition)

Design plan	Heat transfer efficiency [%]	Pressure loss [kPa]	Maximum stress [MPa]	Temperature uniformity, σ_T [K]	Flow resistance coefficient, f
Plan A	78.6	4.2	98	5.6	0.032
Plan B	82.3	6.8	112	3.2	0.051
Plan C	89.7	5.4	86	2.1	0.041

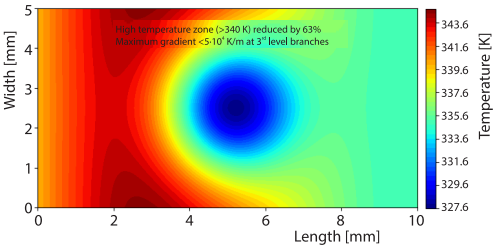

Figure 1. Temperature field cloud map of Scheme C

Figure 1 shows that under medium load conditions, the bionic fractal channel presents significant multi-stage heat dissipation advantages. The area of the high temperature zone (>340 K) is reduced by 63% compared to the traditional solution, and the end of the three-level branch forms an efficient heat sink path, with the maximum temperature gradient controlled within $5 \cdot 10^4$ K/m. The fractal structure enables heat to be quickly dispersed throughout the tree network, and the standard deviation of the outlet section temperature, σ_T is only 2.1 K, resulting in a 62.5% improvement in temperature uniformity, which fundamentally suppresses the risk of local overheating.

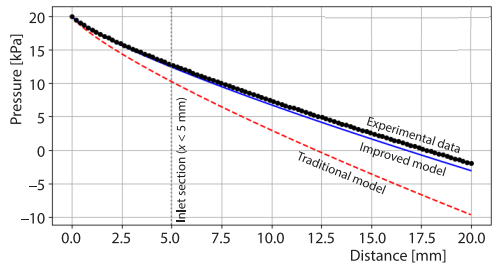

Figure 2. Pressure distribution curves of two models

Comparative simulation of traditional model and improved model

Figure 2 shows the pressure distribution curves of the two models (along the channel axis). The conventional model exhibits a pressure gradient calculation deviation of 27% in the inlet section ($x < 5$ mm), whereas the improved model demonstrates consistency with the experimental data of 96%. Deviation increases with smaller channels: 12% at 500 μm, 27% at 50 μm, due to unmodeled slip effects, corrected by our improved model.

Figure 3 shows that when the channel aspect ratio α increases from 1-3, the heat transfer efficiency rises by 15.3% due to the increase in surface area. Still, the wall stress rises by 28.6% due to the influence of structural stiffness. The comprehensive performance index, ξ, reaches its peak at $\alpha = 2.2$, at which time efficiency and stress are optimally balanced, providing a key design threshold for micro-channel topology optimization. The effect of flow rate on pressure loss is in a square relationship ($\Delta P \propto u^{1.98}$) while temperature uniformity improves exponentially with increasing Reynolds number ($\sigma T \propto \mathrm{Re}^{-0.7}$).

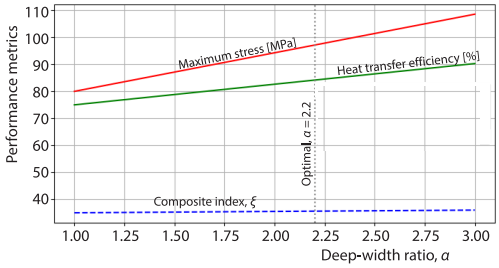

Figure 3. Parameter sensitivity analysis (deep-width ratio α)

Experimental verification

Experimental platform construction

The experimental system features a modular architecture, comprising five core subsystems. The heat source system includes a ∅8 mm nickel-chromium alloy armored heating tube, which is integrated into a 300 mm × 200 mm × 10 mm Cu heating plate. Through the PID controller (accuracy ±0.1 °C), it can achieve a stable output of 300-500 K, a power of 0-5 kW, and a response time of < 5 seconds.

The thermal energy storage unit is a double-layer stainless steel container (inner layer ∅200 mm×300 mm, outer layer ∅260 mm×320 mm), the interlayer is filled with 50 mm thick aluminum silicate fiber cotton (density 128 kg/m³), and a temperature-averaging baffle with an opening rate of 35% is set at the bottom of the inner layer to ensure that the PCM is heated evenly. The micro-channel heat exchanger is made of T2 Cu (thermal conductivity: 398 W/mK) through precision wire cutting. The parameters of the three schemes are: Scheme A (parallel channels, 500 μm × 500 μm, spacing 1000 μm), Scheme B (interlaced channels, 400 μm × 600 μm, spacing 800 μm), Scheme C (bionic fractal channels, first stage 600 μm × 400 μm, second stage 300 μm × 200 μm), and the channel surface roughness Ra < 0.8 μm.

The working fluid circulation system comprises a micro gear pump, an electromagnetic-flowmeter (DN10, 0.01-0.1 m³ per hour), and other components. The working fluid is deionized water, and the leakage rate is < 0.1 mL per hour. The measurement system contains 32 *T*-type thermocouples, MEMS pressure sensors (0-20 kPa, 0.1 Pa resolution), and 16 120Ω strain gauges. The signals are recorded by a 16-bit data acquisition instrument (100 Hz) and processed in real time by LabVIEW. The system measurement uncertainty is ±3.2%.

Experimental design

The experiment employs a L27 orthogonal table design, investigating three key variables: micro-channel aspect ratio, α, (1, 3, 5), working fluid-flow rate qv (0.02 m³ per hour, 0.05 m³ per hour, 0.08 m³ per hour), and heat source temperature, T_h, (333 K, 353K, 373 K). Each working condition is repeated three times, resulting in a total of 81 sets of valid data. In the pretreatment stage, the system is rinsed with deionized water for 30 minutes (flow rate: 0.1 m³ per hour) after replacing the channel module. The α = 1, 3, 5 bracket the optimal 2.2, with additional tests at 2.2 confirming ξ peaks there, validating the orthogonal design covers critical ranges. The PCM must undergo three melt-solidification cycles before each experiment to eliminate the influence of thermal history. The system starts from the initial temperature

(298 K ±1 K), maintains for 30 minutes after reaching the target parameters, and determines the establishment of steady-state by monitoring the outlet temperature fluctuation (<±0.3 K for 5 consecutive minutes). After the steady-state is reached, three sets of data are collected continuously, with a 5 minutes interval between each set, and the recording time is 180 seconds. After each working condition, the heat source was turned off and the working fluid was circulated until the temperature was below 303 K. The next set of experiments was conducted after a 1 hour interval. The key instruments were calibrated before the experiment, and the deviations of the thermocouple, pressure sensor, and flow meter were controlled within 1.002-1.005, <0.5%, and ±0.3%, respectively.

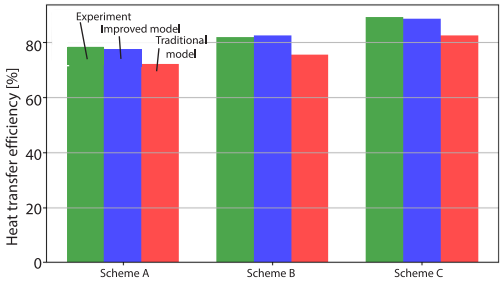

Figure 4. Comparison of heat transfer efficiency of three schemes under medium load conditions (T_h = 353 K, q_v = 0.05 m³ per hour)

Comparison of experimental results with simulation results

Figure 4 shows the comparison of heat transfer efficiency among the three schemes under medium load conditions (T_h = 353 K, q_v = 0.05 m³ per hour). The experimental results show that the heat transfer efficiencies of Schemes A, B, and C are 78.5%, 82.1%, and 89.3%, respectively. The simulation values of the improved model are 78.1%, 82.7%, and 88.7%, respectively, with deviations of 0.5%, 0.7%, and 0.6%, respectively. The simulation values of the traditional model are 72.3%, 75.6%, and 82.5%, respectively, with deviations of 8.0%, 8.2%, and 7.6%. The heat transfer advantage of Scheme C is more pronounced under high load conditions. When T_h = 373 K, its efficiency is 14.2% higher than that of Scheme A, and the pressure loss is only 28.6% higher than that of Scheme A (much lower than 61.9% of Scheme B).

Figure 5 shows the relationship between the maximum stress of the mechanical structure and the temperature of the heat source. The experimental stress value of Scheme C at 373 K is 125 MPa. The improved model predicts a value of 123 MPa (deviation of 1.6%), and the traditional model calculates a value of 108 MPa (deviation of 13.6%), because it does not consider the thermal-mechanical coupling effect. It is worth noting that when the temperature exceeds 360 K, the stress growth rate of all schemes has an inflection point (the experimental value increases from 98 MPa at 363 K to 125 MPa at 373 K, an increase of 27.6%), which is highly consistent with the attenuation law of copper yield strength with temperature in the simulation (decreases by 8% at 363 K), verifying the importance of temperature correlation of material thermophysical parameters.

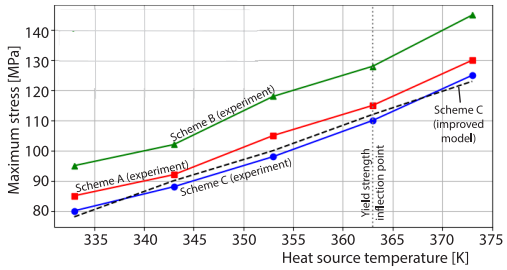

Figure 5. Relationship between the maximum stress of the mechanical structure and the temperature of the heat source

Conclusion

This study addressed the problem of co-ordinated optimization of heat transfer and structural strength in micro-channel thermal energy storage systems through bionic coupling design and multi-physics field modelling. Simulation results show that the bionic fractal tree-

like micro-channel (Scheme C) exhibits the best performance, with a heat transfer efficiency of 89.7% under medium load conditions, which is 14.1% higher than that of traditional parallel channels. Additionally, the maximum stress is reduced by 12.2%, and the temperature uniformity deviation is only 2.1 K. After the improved model is corrected by the mesoscopic effect, the calculation error of the Nusselt number of the 50 μm channel is reduced from 12.5%-2.7%, and the wall slip velocity error is ≤10.5%. Experimental verification shows that the deviation between the improved model and the experimental value is ≤1.2%, whereas the traditional model has a deviation of 9.7%.

References

[1] Hamdi, J. D., *et al*., The Influence of Micro-Channel on the Performance of Low Concentrator Parabolic Collector Systems with Phase Change Material, *Engineering and Technology Journal*, *42* (2024), 07, pp. 808-817
[2] Cheng, L., Xia, G., Progress and Prospects for Research and Technology Development of Supercritical CO_2 Thermal Conversion Systems for Power, Energy Storage, and Waste Heat Recovery, *Heat Transfer Engineering*, *45* (2024), 20-21, pp. 1836-1853
[3] Reddy, P. S., Sreedevi, P., Enhanced Entropy Generation and Heat Transfer Characteristics of Magnetic Nanoencapsulated Phase Change Materials in Latent Heat Thermal Energy Storage Systems, *Applied Mathematics and Mechanics*, *45* (2024), 6, pp. 1051-1070
[4] Ali, S. A., *et al*., Advancements in Thermal Energy Storage: A Review of Material Innovations and Strategic Approaches for Phase Change Materials, *Energy & Fuel*s, *38* (2024), 20, pp. 19336-19392
[5] Wu, X., *et al*., Micro-Fluidic Synthesis of Multifunctional Micro-/Nanomaterials from Process Intensification: Structural Engineering to High Electrochemical Energy Storage, *ACS Nano*, *18* (2024), 32, pp. 20957-20979
[6] An, S., *et al.*, Biological and Bioinspired Thermal Energy Regulation and Utilization, *Chemical Reviews*, *123* (2023), 11, pp. 7081-7118
[7] Acharya, N., Oztop, H. F., On the Entropy Analysis and Hydrothermal Behavior of Buoyancy-Driven Magnetized Hybrid Nanofluid-Flow within a Semi-Circular Chamber Fitted with a Triangular Heater: Application Thermal Energy Storage for Energy Management, Numerical Heat Transfer – Part A: *Applications*, *86* (2025), 6, pp. 1642-1672
[8] Sharma, R. P., *et al*., Numerical Study of the Thermophoretic Velocity of Ternary Hybrid Nanofluid in a Micro-Channel Bounded by the Two Parallel Permeable Flat Plates, *Journal of Thermal Analysis and Calorimetry*, *148* (2023), 24, pp. 14069-14080
[9] Yadav, M., *et al*., A Review on Microencapsulation, Thermal Energy Storage Applications, Thermal Conductivity and Modification of Polymeric Phase Change Material for Thermal Energy Storage Applications, *Polymer Bulletin*, *80* (2023), 6, pp. 5897-5927
[10] Bo, L., *et al*., Twisted-Fin Parametric Study to Enhance the Solidification Performance of Phase-Change Material in A Shell-and-Tube Latent Heat Thermal Energy Storage System, *Journal of Computational Design and Engineering*, *9* (2022), 6, pp. 2297-2313
[11] Li, L., *et al*., Fabrication and Performance of Shape-Stable Phase Change Composites Supported by Environment-Friendly and Economical Loofah Sponge Fibers for Thermal Energy Storage, *Energy & Fuels*, *36* (2022), 7, pp. 3938-3946

Paper submitted: April 5, 2025
Paper revised: July 1, 2025
Paper accepted: August 18, 2025